Environmental Science Processes & Impacts

ROYAL SOCIETY OF CHEMISTRY

PAPER

View Article Online
View Journal | View Issue

Cite this: *Environ. Sci.: Processes Impacts*, 2025, **27**, 992

UV-weathering affects heteroaggregation and subsequent sedimentation of polystyrene microplastic particles with ferrihydrite†

Johanna Schmidtmann, *[a] Hannah-Kristin Weishäupl,[a] Luisa Hopp,[a] Nora Meides[b] and Stefan Peiffer[a]

Microplastic (MP) particles are ubiquitous in aquatic environments where they become exposed to UV-irradiation with subsequent alteration of surface properties. Such particles will interact with naturally occurring colloids being subject to processes like heteroaggregation that affect both MP surface properties and their removal rates from the water column. In this study, we investigated heteroaggregation and subsequent sedimentation of 1 μm polystyrene (PS, pristine and UV-weathered) with ferrihydrite (Fh), an iron (oxy)hydroxide commonly found in nature. Heteroaggregation of pristine PS with Fh was controlled by electrostatic attraction. At neutral pH values, strong heteroaggregation was observed which led to the sedimentation of almost all PS particles. UV-weathering of PS led to lower negative surface charge, decrease of particle size, and formation of degradation products. Changes in surface properties of PS resulted in a different aggregation behavior with Fh. With increasing weathering time, the isoelectric point (pH_{IEP}) of suspensions with PS and Fh shifted to lower pH values. Furthermore, we observed aggregation and subsequent sedimentation of weathered PS and Fh for a wider pH range (pH 3–7) compared to pristine PS (pH 6.5–7.5). We attribute this observation to increased surface reactivity of PS due to the formation of functional groups on the surface through UV-weathering. In addition, degradation products (*e.g.* oligomers) formed during weathering might have also interacted with PS and Fh and therefore further affected the surface properties of the particles. Overall, UV-weathering but also interactions of MP particles with environmental particles cause changes of MP surface properties, which influence its environmental behavior in water and might lead to a removal from the water column and accumulation in sediments.

Received 31st October 2024
Accepted 27th February 2025

DOI: 10.1039/d4em00666f

rsc.li/espi

Environmental significance

When microplastic particles enter aquatic environments, they will become exposed to UV-weathering, leading to changes in surface properties, composition and size. Concurrently, such particles will get into contact with natural constituents, driving heteroaggregation and subsequent removal of microplastic particles from the water column upon sedimentation. This work investigates the aggregation and sedimentation of pristine and UV-weathered polystyrene particles with ferrihydrite, a naturally occurring iron (oxy)hydroxide. Our findings suggest that UV-weathering of polystyrene intensifies the interactions with ferrihydrite, potentially reducing the residence time of microplastic particles in the water column and increasing its accumulation in sediments. This knowledge is crucial for understanding the environmental behavior of microplastic, particularly in terms of its distribution in the environment and its long-term ecological effects.

1. Introduction

Microplastic particles (MP, plastic fragments < 5 mm) have been found in nearly every environmental compartment, such as marine and coastal environments,[1,2] freshwaters,[3,4] soils,[5,6] air,[7,8] and even at remote places like Antartica.[9] Their widespread distribution has raised concerns about the effect these particles may exert on the functioning of aquatic ecosystems.[10–12] A key requirement for the evaluation of the risk that MP particles pose to the environment and its organisms is a thorough understanding of their transport and fate. In aquatic environments, MP particles are expected to interact with various natural particles and colloids, such as natural organic matter (NOM),[13–15] mineral particles[16–18] or biogenic particles[19–21] which may influence the surface and transport properties of MP particles and eventually lead to heteroaggregation. As an example, coating with NOM, such as humic acids or polysaccharides, may stabilize MP particles in the aqueous phase on the one hand by enhancing

[a]*Department of Hydrology, University of Bayreuth, Bayreuth Center for Ecology and Environmental Research (BayCEER), Germany. E-mail: j.schmidtmann@uni-bayreuth.de*

[b]*Department of Macromolecular Chemistry I, University of Bayreuth, Germany*

† Electronic supplementary information (ESI) available. See DOI: https://doi.org/10.1039/d4em00666f

electrostatic repulsion and steric hindrance.[22–24] On the other hand, NOM may also lead to destabilization of colloidal MP upon bridging or reversing surface charge.[14,15,22,23,25] Interactions of MP particles with environmental particles appear to be predominantly controlled by electrostatic attraction or repulsion forces and charge neutralization is mainly responsible for heteroaggregation[15,16,18,25] which has been shown to increase the sedimentation rate of MP particles.[16,19–21]

Until now, most studies investigating the interactions of MP particles with environmental particles have been conducted with pristine MP particles.[13,14,16–19] In the environment, however, MP particles are exposed to various weathering processes, including UV-irradiation from the sun. Zhang *et al.* showed that UV-weathered polystyrene (PS) nanoparticles, unlike the pristine material, interacted with clay minerals and the adsorption of PS nanoparticles onto iron oxides increased with increasing UV-weathering time.[26] UV-induced weathering can lead to changes in chemical composition, surface charge, and mechanical properties of MP particles,[27–29] all of which can affect their aggregation behavior. The formation of oxygen-containing functional groups on the MP surface (*e.g.* carboxyl, peroxy, and keto groups)[27] may increase the number of active surface sites allowing for additional interactions *via* hydrogen bonding or ion-complexation.[26,30] Overall, these processes increase the hydrophilicity and intensify attractive forces between weathered MP particles and charged environmental particles.[26,30]

Although the importance of UV-weathering of MP particles for interactions with environmental particles and colloids has been demonstrated,[26,30] research on the effect of UV-weathering on the heteroaggregation and its effect of sedimentation properties of microplastic particles is still missing.

In this study, we examined the pH-dependent heteroaggregation and subsequent sedimentation of UV-weathered PS particles and ferrihydrite (Fh), a ferric iron (oxy)hydroxide commonly found in the environment.[31–33] In previous work we could show that Fh not only promotes heteroaggregation but also sedimentation of PS particles.[16] At neutral pH, heteroaggregation between PS and Fh led to almost complete sedimentation of PS particles within just one day.[16] In order to test how heteroaggregation and sedimentation of PS is affected by UV-weathering, we conducted the experiments in this study with PS particles (1 μm), which were pre-weathered in an accelerated UV-weathering chamber for different exposure times. We hypothesize that UV-weathering of PS will render the MP surfaces more reactive and thus intensify the interactions with Fh.

2. Material and methods

2.1 Material

For the experiments, we used spherical non-functionalized PS particles (diameter 1.01 ± 0.03 μm microParticles GmbH, Berlin, Germany). According to the manufacturer, the particles' surfaces contain sulfate from the manufacturing process. The suspension of 10% w/v was diluted to a stock solution of 100 mg L^{-1} with ultrapure water (18.2 MΩ cm). Aggregation and sedimentation experiments were done with a PS concentration of 10 mg L^{-1}. We selected a concentration of 10 mg L^{-1} based on two considerations. First, the concentration needed to be high enough for reliable detection with our measurement techniques and second, this value allows for comparison with previous studies on microplastic interactions and aggregation. The chosen concentration falls within, or in many cases below, the range reported in comparable studies (4–160 mg L^{-1}).[13–18,23,34,35] The synthesis of Fh followed the method outlined by Cornell and Schwertmann[36] and previously described in detail by Schmidtmann *et al.*[16]

2.2 UV-weathering

For UV-weathering experiments of PS particles, we used an UVACUBE 400 irradiation chamber for solar simulation, equipped with a SOL500 lamp (both Dr. Hönle AG, Germany). Further information on the weathering chamber can be found in the ESI (Tables S1, S2 and Fig. S1).† Based on data of the manufacturer, we calculated the acceleration factor of the weathering chamber compared to average irradiation in Germany. The irradiance was 10-fold enhanced (Tables S1 and S2†). Accelerated UV-weathering in a controlled laboratory setting is a common approach to simulate natural UV exposure, enabling the study of microplastic degradation within a feasible timeframe while ensuring real-world relevance.[27–29,37] 200 mL of 100 mg L^{-1} PS stock suspensions (diluted in ultrapure water) were added into 250 mL quartz beakers, closed off with a quartz glass sheet secured with 4 metal clips (Fig. S2†) and placed in the chamber for periods between 0–960 h. For aggregation and sedimentation experiments, PS samples with weathering periods of 0, 48, and 96 h were used. Samples weathered for periods longer than 96 h were only used for the quantification of carbon after each weathering step (see Section 2.4.2). To ensure that all samples received consistent irradiation intensities regardless of their position in the irradiation chamber, we rotated the position of the sample beakers every 48 hours. As the beakers were not sealed gas tight (to allow oxygen supply for the photochemical oxidation) the evaporated amount of water was refilled with ultrapure water every 48 h. After the respective irradiation time was reached, the sample was stored at 4 °C in airtight glass bottles in the dark.

2.3 Sedimentation experiments

Sedimentation experiments were conducted in narrow glass vessels (inner diameter ≈ 16 mm, vessel height ≈ 65 mm, water column height ≈ 50 mm for a volume of 10 mL). Samples containing either pristine or UV-weathered PS (10 mg L^{-1}) and Fh (10 mg L^{-1}) were prepared under room temperature and ambient pressure. The pH of the samples with a total volume of 10 mL was adjusted to values between 3 and 11 by adding HCl or NaOH. A constant ionic strength of 10 mM was established by addition of adequate amounts of NaCl. Subsequently, the samples were shaken to achieve complete mixing and then allowed to react for one day. This period was chosen as previous work showed that the relevant sedimentation patterns were already observed after one day.[16] Afterwards we carefully removed the upper 8 mL of the samples with a pipette and transferred them to a second sample vial without disturbing any

settled particles in the lower 2 mL of the sample. In the following, we will refer to the lower 2 mL of the sample as "sediment" and to the upper 8 mL of the sample as "solution" (Fig. S3†). The sediment phase was diluted with 6 mL ultrapure water to a volume of 8 mL.

As reference, we analyzed the sedimentation of PS_{0-96h} in the absence of Fh. Reference samples were prepared under identical conditions as explained above (pH 3–11, ionic strength of 10 mM) and same PS concentration but without Fh.

2.4 TOC analysis

Total organic carbon (TOC) analysis was done to (i) determine the amount of PS that sedimented after reaction with Fh (as described in Section 2.3) and (ii) to determine the amount of TOC and dissolved organic carbon (DOC) in PS suspensions after UV-weathering.[38]

2.4.1 Sedimentation. To determine the amount of PS that sedimented in presence or absence of Fh, the carbon content was measured in the sediment as well as in the solution of each sample. A TOC-L-Analyzer (Shimadzu, Japan) was used and 10 mg L^{-1} Fh were added to all samples prior measurement as the addition clearly improved the recovery of PS.[38] Approx. 10 minutes prior to analysis, samples were acidified with 2 M HCl and pre-treated in an ultrasonic bath for approx. 5 minutes to dissolve any possible aggregates. To prevent sedimentation of the particles in the sample vial during measurement, the samples were placed on a magnetic stirrer instead of using the auto-sampler of the instrument. Each sample was measured twice and the mean value was calculated. If the relative standard deviation of the first two measurements was greater than 2%, a third sample was taken.

2.4.2 Quantification of TOC and DOC after weathering. To investigate whether or not the PS samples experienced a mass loss during UV-weathering, we conducted TOC-measurements of PS samples after weathering periods of 0–960 h. TOC-analysis was performed in triplets for (i) unfiltered samples and (ii) samples which had been filtered through 0.45 μm (Chromafil Xtra PA-45/25, Macherey-Nagel GmbH & Co. KG, Germany). The unfiltered samples were used to determine the total amount of carbon in each sample. The filtered samples provided information about the quantity of carbon that was present as dissolved substances or fragments <0.45 μm. As the size fraction of carbon smaller than 0.45 μm is usually termed "DOC", we also use this term in our study. However, please note that even though it contains the word "dissolved", it also accounts for fragments, small enough to pass through the 0.45 μm filter. The unfiltered sample at 0 h UV-weathering (PS_{0h}) was set as reference for total carbon concentration (TOC_{0h}) for samples that had been exposed to UV-irradiation. Based on the value of TOC_{0h}, the percentage of TOC and DOC for each weathering period was calculated.

2.5 Determination of zeta potential and hydrodynamic diameter

To investigate surface charge and aggregate size of PS, Fh, and samples containing both particle types, we determined zeta potential and *z*-averaged hydrodynamic diameter using a Zeta-Sizer Nano ZS (Malvern Panalytical, Germany) by Laser Doppler Electrophoresis or Dynamic Light Scattering (DLS), respectively. All measurements were conducted at a concentration of 10 mg L^{-1} for both PS and Fh, while the pH was adjusted to values ranging from 3 to 11, and the ionic strength was maintained at 10 mM by adding NaCl. Prior to the ZetaSizer analysis, the samples were briefly shaken to re-suspend any sedimented aggregates. A subsample of approximately 1 mL was examined at 25 °C using a folded capillary zeta cell (DTS1070, Malvern Panalytical, Germany). Each sample underwent four measurements of electrophoretic mobility, and the results were reported as the average of these measurements with standard deviations. Electrophoretic mobility was converted into zeta potential by use of the Smoluchowski equation as provided by the instrument.

2.6 Scanning electron microscopy

SEM analysis was performed to investigate the aggregation of PS and Fh. Sample preparation was the same as described for ZetaSizer measurements. Then, 4 μL of the suspension were dropped onto a glow-discharged carbon-supported TEM copper grid (S160 Plano, Germany) and dried under ambient conditions. The samples were coated with a thin layer of platinum by a Cressington 208 HR sputter coater. SEM images were recorded using secondary electron detectors on a Zeiss ULTRA PLUS (Carl Zeiss Microscopy GmbH, Germany).

3. Results and discussion

3.1 Ferrihydrite characterization

Zeta potential measurements of Fh showed characteristic values for this material (Fig. S4A†). The isoelectric point (pH_{IEP}) was located at pH 8, lying in the range of values reported in the literature.[16,39,40] For lower pH values, the zeta potential values were positive and for higher pH values negative. For pH < 5.8, Fh particles exhibited nanometer-scale dimensions (Fig. S4A†) and some of the iron (oxy)hydroxide might even have been present as dissolved iron. The count rates for those samples might not be sufficient for reliable light scattering measurements. Consequently, careful consideration should be given to the numerical value of zeta potential and hydrodynamic diameter measurements obtained from Fh samples with pH values < 5.8. Nevertheless, the measurements provided a reasonable estimate for the pH_{IEP}. As expected, maximum homoaggregation of Fh was found at the pH_{IEP}, where repulsive forces between the particles are lowest (Fig. S4B†). For samples with pH values between 6 and 10, aggregation and sedimentation could be observed as a characteristic red-brown sediment at the bottom of the sample vial.

3.2 Characterization of UV-weathered PS

3.2.1 Formation of surface defects and holes on the surface. UV-weathering had a strong impact on particle size, shape, and surface characteristics. Pristine PS particles were monodisperse and spherically shaped with a smooth surface

(Fig. S5†). With increasing exposure to UV-weathering, the particle surface became rougher, the particle size decreased and the size distribution between the particles increased (Fig. 1B and additionally Fig. S6† showing SEM images of PS_{48h}–PS_{480h}). Most notably, for weathering times longer than 96 h, we noticed cavities in PS particles (Fig. 1B and S6D–I†). Some particles seemed to become hollow in the center with distinct pierced, or wrinkled surfaces. Similar hollow structures were observed in previous research with spherical 5 μm PS particles.[41] However, to the best of our knowledge, this effect has not yet been observed for plastic particles other than spherical PS beads in the micrometer size range. The mechanism behind the hollowing process remains unclear but may be related to the fabrication process. With increasing weathering time, the heterogeneity of size and shape increased, as we observed varying stages of degradation for the same sample. Some particles showed completely altered surfaces and a crumpled shape, while other particles were smooth and spherical with no visible difference to pristine particles. After 480 h of UV-weathering, no spherical particles were observed anymore. Instead, we found clumps of material, presumably made up of degradation products of the PS particles (Fig. S6K and L†).

3.2.2 UV-weathering results in a decreased negative surface charge. The surface charges of PS particles were negative for all analyzed weathering time steps (0–96 h) over the complete pH range between 3 and 11 (Fig. 1A). The values of pristine particles (PS_{0h}) ranged from −52.9 mV (pH 3) to −96.7 mV (pH 11), indicating strong repulsion between PS particles and therefore a stable dispersion. This was confirmed by sedimentation experiments of PS in the absence of Fh showing only minor sedimentation and no major differences over the tested pH range between 3 and 11 (Fig. S7†).

Interestingly, the initial surface charge of the pristine material used in our study was clearly more negative compared to previous studies.[26,42–44] The high negative charge of our PS particles is most likely caused by sulfate groups due to the manufacturing process. With increasing weathering time, PS exhibited less negative zeta potential values in analogy with observations made in UV-weathering studies with 2 μm PS.[45] Most previous studies, however, found increasing negative zeta potential values for UV-weathered PS (diameter between 50 nm and 1 μm)[26,42,43] or polyethylene (PE) particles (diameter 0.4 μm).[44] The increase in negative surface charge of weathered particles compared to pristine particles was attributed to functional groups formed on the MP surface during UV-weathering, *e.g.* carboxyl groups.[26,42,44] It is highly probable, that this also happened during our weathering experiments, but became masked by the high initial potential.

Notably, even though the MP particles in previous studies[26,42–44] developed higher negative zeta potentials with UV-weathering, the final values were still less negative than our pristine and UV-weathered PS particles. We therefore propose a combination of two processes taking place for the analyzed 1 μm PS during UV-weathering: (i) cleavage of negatively charged sulfate groups led to a reduction of negative surface charge,[42] while (ii) negatively charged oxygen-containing functional groups were simultaneously formed by UV-irradiation. The net effect was a slight shift to a less negative surface charge compared to the initial charge of the pristine particles (Fig. 1A). Unfortunately, we were not able to quantify the amount of leached sulfate in the solution after different weathering periods by use of ion chromatography, with concentrations being below the detection limit (0.1 mg L^{-1}).

3.2.3 UV-weathering converts PS beads to smaller sized fragments. With increasing weathering time, the carbon concentration in the PS suspensions decreased (Fig. 2). Before weathering, the TOC concentration of the unfiltered PS_{0h} sample (100 mg L^{-1}) was 88.0 ± 3.0 mg L^{-1} matching well with the TOC concentration expected based on the carbon content in PS (92.3 mg L^{-1}, PS-monomer: C_8H_8).

The strongest decrease of TOC was observed between 48–240 h. After 300 h of UV-weathering, only approx. 10% of the initial TOC concentration remained in the samples. This indicates that a substantial portion of carbon (and thus PS) was removed during UV-weathering, likely in gaseous form, as it could not be detected in the solution anymore.

For DOC, firstly an increase was observed as the 1 μm particles degraded to smaller particles. The DOC concentration peaked at 144 h of weathering and decreased again thereafter. The concentrations of TOC and DOC were nearly the same for

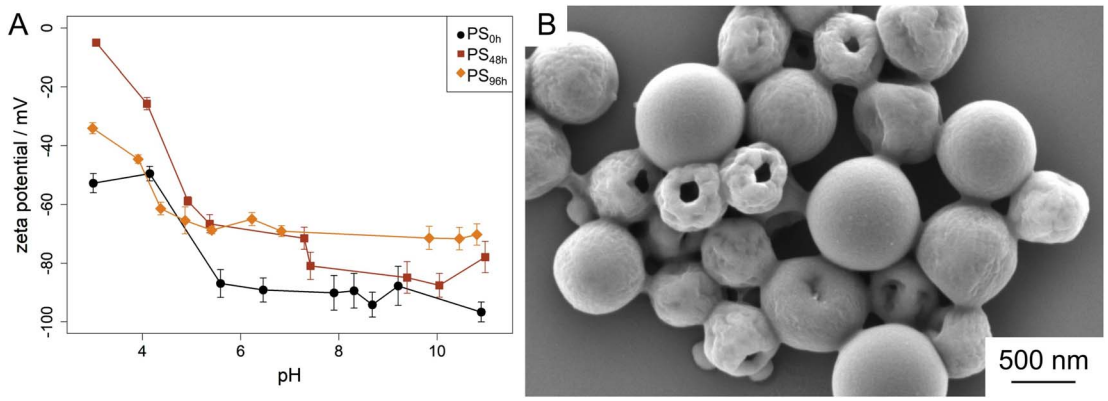

Fig. 1 (A) Zeta potential values for pristine PS samples (PS_{0h}) and PS samples exposed to UV-weathering for 48 and 96 h. (B) SEM image of PS particles weathered for 144 h.

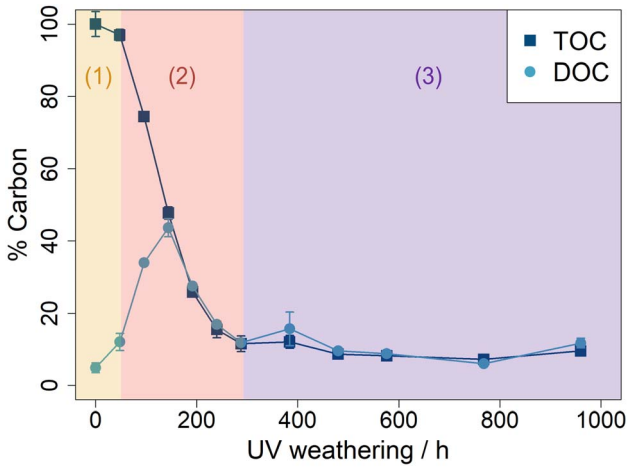

Fig. 2 Percentage of total (TOC) and dissolved organic carbon (DOC) in PS samples after UV-weathering (0–960 h). DOC accounts for dissolved material and all fragments <0.45 μm. The percentage was calculated based on the initial carbon concentration in samples before weathering (PS_{0h}). The numbered, colored areas are attributed to the different degradation stages: (1) initiation, (2) propagation, and (3) termination.

weathering times larger than 144 h indicating that all remaining PS particles must have been degraded to fragments smaller than 0.45 μm or to truly dissolved substances. This was supported by measurements of electrical conductivity (Fig. S8†). The initially very low conductivity of 100 mg L^{-1} PS_{0h} suspension (2.7 μS cm^{-1}) increased with UV-weathering to a maximum of 93.8 μS cm^{-1} for PS_{144h}. For longer weathering times, the conductivity decreased again, just as observed for the DOC concentration.

The transformation of 1 μm PS particles to smaller fragments, DOC, and potentially into gas was also visually seen by color and turbidity of the samples. Before UV treatment, the PS suspensions were turbid due to suspended PS particles. With increasing UV-weathering, the suspension cleared out and after 192 h, it visually appeared as a clear solution (Fig. S2†).

The stepwise fragmentation of PS including CO_2 formation has previously been reported for UV-weathered PS particles, and was interpreted as degradation of initially formed fragments that are further degraded to water-soluble organics with increasing UV-weathering time.[37,46] Ward *et al.*[46] measured the DOC concentration in pristine and weathered PS suspensions after filtration. DOC concentrations strongly increased after UV-weathering. They concluded that UV-weathering could partially oxidize PS to DOC and a certain fraction even further to CO_2.[46] The observed loss of mass in carbon and consequently in PS in our experiments might therefore also indicate a transformation of PS into gaseous components like CO_2. Unfortunately, our experimental setup did not allow quantifying those potentially formed gases.

The results obtained from Ward *et al.*[46] cannot directly be compared with those from our experiments as various experimental settings differed. UV chambers and irradiation intensity were different, filter sizes for DOC differed (0.45 μm *vs.* 0.7 μm [46]) as well as the PS used (1 μm PS beads *vs.* 192 μm thick PS film[46]). Nevertheless, our observation of temporary increase in DOC and continuous PS mass loss during UV-weathering can be well described with a previously established model for UV based degradation occurring in three stages.[30] In the first initiation stage, chain scission of polymer chains occurs accompanied by the formation of radicals (*e.g.* R•, RO•, ROO•) and reactive oxygen species (ROS), such as hydroxyl (•OH) or superoxide ($O_2^{\bullet -}$) radicals takes place.[30] In the following propagation stage, highly active radicals promote self-catalyzed reactions[30] and the analyzed PS particles degrade further into smaller particles, dissolved species and gaseous components. Eventually, the termination stage is marked by the total mineralization of PS particles.[30] However, for the analyzed 1 μm PS particles, approx. 10% of the initial TOC remained in the sample and were therefore not transformed into gas with the duration of the experiments (Fig. 2).

For UV exposure times of 144 h and longer, almost all PS was recovered in the fraction <0.45 μm and approx. 50% of the carbon presumably degassed from the sample (Fig. 2). Therefore, we conducted heteroaggregation and sedimentation experiments only for the time steps of 0, 48 and 96 h.

3.3 Heteroaggregation and subsequent sedimentation of pristine and UV-weathered PS with Fh

3.3.1 Electrostatic interactions control aggregation of pristine and shortly weathered PS with Fh. The observations made for PS_{0h} confirmed results of previous work demonstrating that aggregation of pristine MP particles and iron minerals is controlled by electrostatic attraction.[16,26,44] At acidic pH values, the negatively charged PS particles became coated with positively charged Fh nanoparticles,[16] which then led to charge reversal at the PS surfaces from negative to positive (Fig. 3A).[16] Under these conditions, no larger aggregates can be formed, since the coated PS particles tend to repel each other due to the positively charged Fh nanoparticles on their surface (Fig. 3A and B).[16] At neutral pH values, the negatively charged PS particles were also coated with Fh.[16] However, as the surface charge of the heteroaggregates was almost neutral at this pH range, it allowed formation of larger heteroaggregates up to several micrometers (Fig. 3B).[16] At alkaline pH values, both particle types are negatively charged, repel each other, and therefore stay separated in suspension.[16] As a consequence, two peaks in electrophoretic mobility were identified reflecting two distinct zeta potentials (Fig. S9†) that refer to two particle fractions. The lower values (∼−80 mV) can be attributed to pristine PS particles while the higher values (∼−10 mV) correspond to values measured for Fh alone (Fig. S10A†).[16]

In accordance to previous findings, heteroaggregation resulted in sedimentation of PS particles.[16,19,20,35,47–49] At neutral pH, where we observed maximum heteroaggregation, we also found maximum sedimentation of PS particles in the presence of Fh (Fig. 3C). Approx. 85% of the initially added amount of PS particles was detected in the sediment at pH 6.8 after one day of settling. Contrary, at pH values at which no increase in aggregate size was observed, also no major sedimentation of PS particles was found (Fig. 3B, C and S7†).

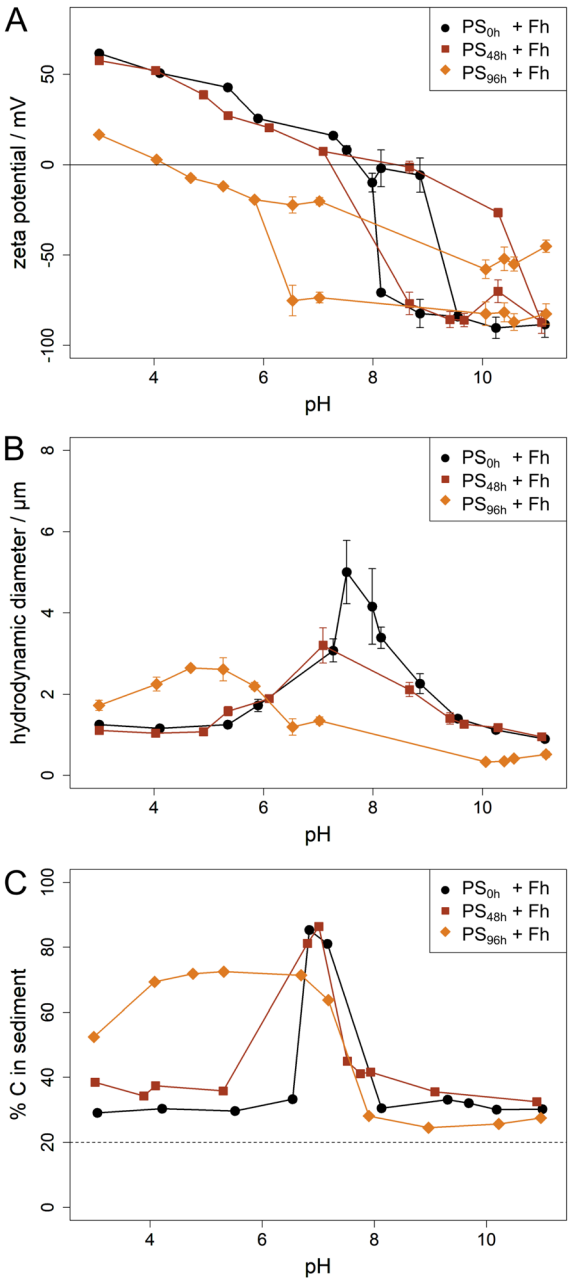

Fig. 3 (A) Zeta potential values and (B) hydrodynamic diameter of samples with (UV-weathered) PS and Fh after a reaction time of one day. (C) Sedimentation of (UV-weathered) PS in the presence of Fh: percentage of carbon (% C) found in the sediment after a settling time of one day. In a well-mixed dispersion, where no sedimentation takes place, 20% of the total PS in the sample (dashed line) should be found in the sediment due to the experimental setup (Fig. S3†).

The shortest exposure time to UV-weathering of PS particles (48 h) had minor influence on the heteroaggregation and sedimentation behavior with Fh. Zeta potentials were rather similar to pristine samples and only the maximum aggregate size decreased slightly (Fig. 3A and B). SEM images of those samples showed a similar pattern compared to reaction of pristine samples with Fh:[16] PS_{48h} particles were covered with a thin Fh coating at acidic pH and strong heteroaggregation of PS_{48h} and Fh took place at neutral pH (Fig. 4A and B). Altogether, the observations suggest, that similar to the pristine samples, heteroaggregation of PS_{48h} and Fh was dominated by electrostatic attraction in this initial weathering phase. Furthermore, as in the presence of pristine samples, maximum sedimentation was found at pH 7 with approx. 85% of the carbon being detected in the sediment after one day. At pH values at which no larger heteroaggregates between PS_{48h} and Fh were formed, no increased sedimentation took place (Fig. 3B, C and S7†).

3.3.2 Contribution of specific interactions to heteroaggregation of PS with Fh after extended UV-weathering time. Compared to the early stage of weathering (0–48 h), exposure of PS particles to an extended weathering period (96 h) led to clearly differing patterns of aggregation with Fh. Similarly to the short weathering period, the tendency of decreasing zeta potential with increasing pH was also observed under these conditions. However, the range of zeta potentials measured over the entire pH range was distinctly smaller for suspensions containing PS particles irradiated for 96 h (+16 to −87 mV) compared to those that experienced a shorter UV exposure time (0–48 h) (+60 to −90 mV) (Fig. 3A). At low pH values, the particle mixture no longer exhibited the highly positive values observed in the initial weathering phase but changed to weakly positive or even negative values close to zero. Also, the pH_{IEP} in suspensions containing PS_{96h} particles and Fh was shifted to a lower, acidic pH value of approx. 4 (Fig. 3A). Thereby, the pH range at which maximum heteroaggregation of PS_{96h} particles and Fh occurred (as indicated by the maximum in hydrodynamic diameter) was also shifted to lower pH values, however, with a lower maximum aggregate size compared to pristine particles (Fig. 3B).

The strong change in the heteroaggregation pattern of PS_{96h} particles with Fh compared to $PS_{0–48h}$ particles with Fh cannot be explained solely by the observed decrease in negative surface charge of PS particles with increasing weathering time (Fig. 1A). Therefore, we propose that further interaction forces were involved in driving heteroaggregation between PS_{96h} particles and Fh.

Previous research has demonstrated that due to the formation of oxygen-containing functional groups on the MP surface upon weathering, interaction forces other than electrostatic attraction may become active, *e.g.* hydrogen bonding or ligand exchange.[26,30] As a consequence, UV-weathered (negatively charged) PS nanoparticles were found to be absorbed onto negatively charged minerals despite electrostatic repulsion.[26] Moreover, the formation of degradation products during UV-weathering, which we partly determined as DOC, indicated a shift in the size spectrum of PS_{96h} particles. It has been demonstrated that weathering of MP particles generally leads to an increase in specific surface area, which is accompanied by an increase in the number of surface sites with different properties compared to the pristine particles.[50,51] In fact, Meides *et al.*[27] demonstrated the formation of surface functional groups. Hence, weathering results in the formation of particles with a surface composition containing surface sites in larger quantity and in different quality as compared to those of the pristine

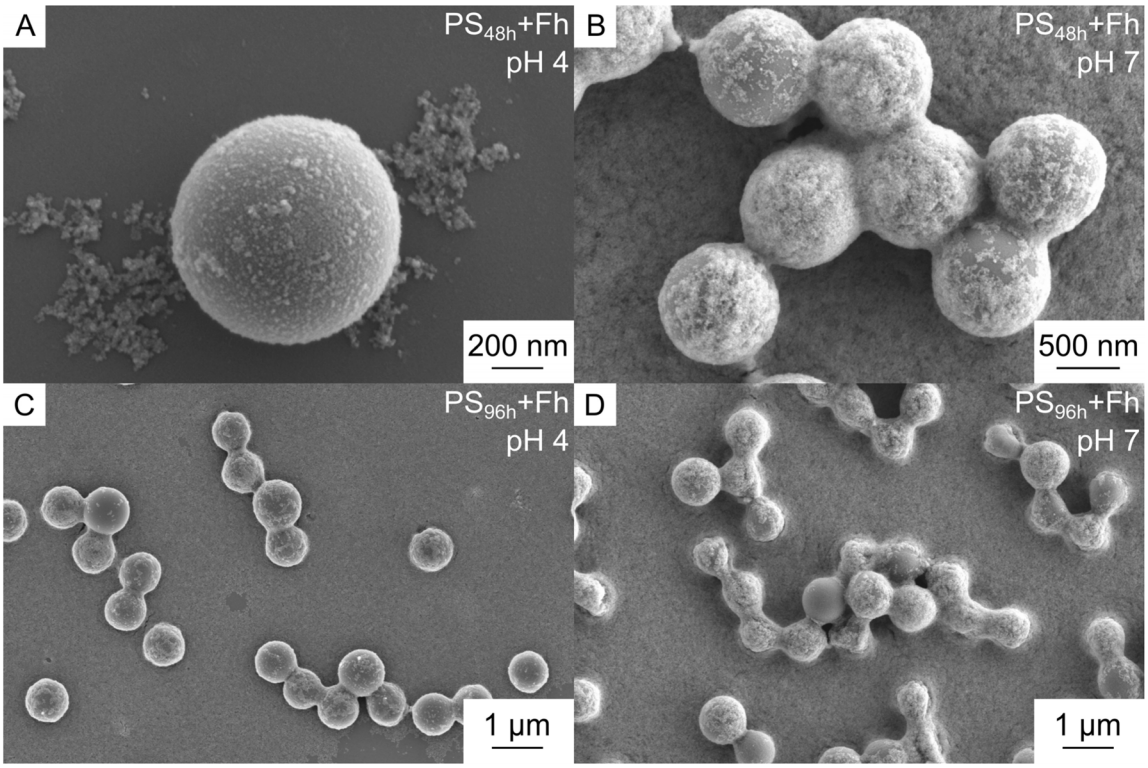

Fig. 4 SEM images of UV-weathered PS and ferrihydrite (Fh) after one day reaction time. For PS_{48h}, a thin ferrihydrite coating was observed at pH 4 (A) and at pH 7 strong heteroaggregation between PS and Fh (B). For PS_{96h}, heteroaggregation with Fh was observed at acidic as well as neutral pH values (C and D).

particles. Such properties may have additional effects on the heteroaggregation process. The highest DOC concentrations were determined for PS particles that were exposed to weathering between 96 h and 192 h (Fig. 2). Hence, the complexity of the composition of the sample containing PS_{96h} particles increased compared to that containing $PS_{0–48h}$ particles. Not only PS particles (with altered properties due to weathering), but additionally, very small (filterable) particles and even truly dissolved organic molecules (*e.g.* polymer fragments with carboxylic acid end groups[52]) formed during weathering may have interacted with Fh, thereby stimulating aggregation. Additional experiments confirmed the hypothesis of interactions between Fh and MP-derived DOC (detailed information provided in ESI Section S1†).

We therefore propose that the formation of heteroaggregates between PS_{96h} particles and Fh at acidic pH (Fig. 3A, B and 4C, D) was not simply caused by interactions between negatively charged PS_{96h} particles and positively charged Fh particles alone, but by additional interactions of these particles with degradation products formed during UV-weathering (and partly recovered as DOC fraction). As a consequence, PS_{96h} particles that had experienced only weak weathering effects, became coated with Fh. The now positively charged surfaces of these particles further interacted with the negatively charged smaller DOC components formed upon PS degradation (Fig. S11†), thereby reducing the net surface charge and allowing for aggregation of PS_{96h} particles coated with Fh-DOC-particles at acidic pH values.

Hence, maximum aggregation of PS_{96h} and Fh was observed in this pH range. These considerations are underpinned by SEM images showing aggregates of several PS particles (Fig. 4C). Compared to samples with shorter UV exposure times (0–48 h), the maximum heteroaggregate size of PS_{96h} with Fh was smaller (Fig. 3B). We attribute this to two factors: firstly, the PS particle size decreases with increasing weathering time. Secondly, the particle size of Fh alone differed strongly between the pH values (Fig. S4B†). Whereas homoaggregation of Fh was observed at neutral pH, resulting in particle sizes of a few micrometers, the Fh particles at acidic pH range were considerably smaller (Fig. S4B†). Hence, the different particle sizes of Fh at different pH ranges probably contributed to the different maximum heteroaggregate sizes observed for heteroaggregation of Fh with pristine PS compared to heteroaggregation with PS_{96h}.

As heteroaggregation is driving sedimentation of MP particles,[16] the shift in the pH-range in which heteroaggregation was observed also influenced the sedimentation rate of PS_{96h} in the presence of Fh. Instead of a clear maximum at neutral pH (as observed for PS_{0h} and PS_{48h}), we found maximum sedimentation rates over a pH range between 3 and 7 (Fig. 3C). With 70% of the carbon being recovered in the sediment, the maximum sedimentation rate was lower compared to pristine particles. The decrease in maximum sedimentation rate of PS_{96h} in the presence of Fh can on the one hand be explained by the composition of the heteroaggregates and the smaller aggregate size. As explained above, the maximum heteroaggregate size of pristine PS with Fh was clearly larger compared to PS_{96h} with Fh,

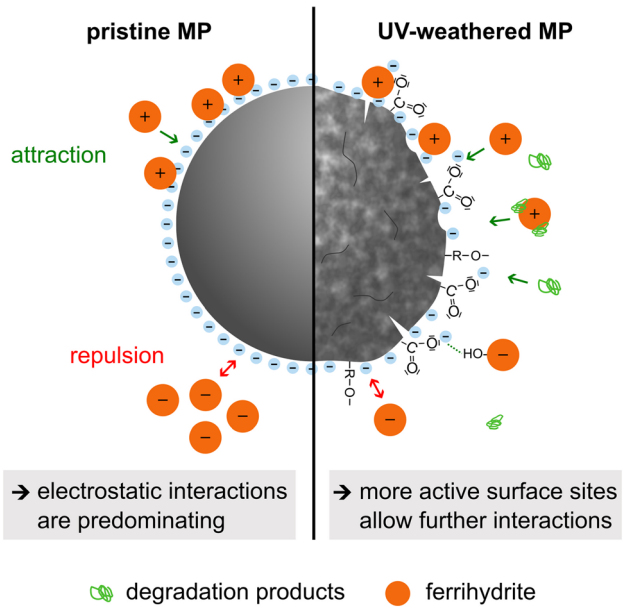

Fig. 5 Conceptual model representing the different interactions of pristine and UV-weathered PS particles with Fh. For pristine MP particles (left), the interactions with Fh are predominated by electrostatic interactions. With increasing UV-weathering (UV-weathered MP, right), more active surface sites form on the MP surface, enabling further interactions (*e.g.* hydrogen bonding) with Fh. Additionally, MP degradation products might also interact with Fh or the MP particles.

likely due to the larger particle/aggregate size of Fh at neutral pH range compared to acidic pH values. On the other hand, with increasing weathering, the degradation of PS particles to smaller fragments and dissolved substances is proceeding. Dissolved substances that were not involved in aggregation with PS_{96h} or Fh particles likely remained in the solution and thus did not contribute to the carbon found in the sediment.

However, even though the sedimentation rate slightly decreased, the pH range at which strong sedimentation of PS_{96h} particles in the presence of Fh was observed, was clearly larger (pH 3–7) compared to pristine samples (pH 6.5–7.5). Hence, UV-weathering of PS allowed intensified interactions with Fh, which resulted in sedimentation taking place over a broader pH range.

At neutral and alkaline pH (pH 6–11), a splitting of zeta potentials into two curves was observed for measurements performed after 96 h weathering (Fig. 3A). For PS exposed to a weathering time of 0 and 48 h, the split curves matched very well those curves obtained from samples containing either Fh only or PS only (Fig. S10A and C†) indicating the occurrence of two domains of particles with different zeta potentials. However, for the longer UV-weathering period, zeta potential values matched only the lower zeta potential curve for pure PS, while the upper curve was located in between the curves of pure PS and pure Fh (Fig. S10E†). This observation suggests that the surface charge of Fh was reduced in the neutral and alkaline pH range, presumably by adsorption of PS degradation products, which were partly recovered as DOC (Section S1†). On the other hand, some Fh particles might have adsorbed onto PS_{96h}. Even though both particles were negatively charged at alkaline pH, weathering-induced oxygen-containing functional groups on PS surfaces might have promoted interactions *via* hydrogen bonding.[26] Hence, a partial adsorption of Fh onto PS_{96h} increased the net surface charge and might explain the zeta potential curve with values in-between unreacted Fh and PS_{96h}.

The occurrence of two classes of particles causing the observed splitting of zeta potentials was corroborated by SEM measurements. At neutral pH, some PS_{96h} particles were strongly coated by Fh and aggregates of several particles occurred (Fig. 4D). At the same time, other PS_{96h} particles remained almost uncoated. Hence, UV-induced changes of PS properties (*e.g.* size, shape, surface charge, composition) resulted in a more heterogeneous mixture of PS. This led to a greater variety of interactions with Fh, allowing adsorption and aggregation processes to take place over a broader pH range compared to pristine particles.

Conclusion

In our study, we demonstrated that UV-weathering stimulates heteroaggregation and sedimentation of PS with iron (oxy) hydroxides at acidic and neutral pH values. UV-weathering led to alteration of PS surface properties, strong fragmentation, and degradation of the particles. The increased reactivity of the PS surface due to UV-weathering, and the formation of degradation products triggered heteroaggregation and subsequent sedimentation over a broad pH range. The different interactions between pristine and UV-weathered MP particles with Fh are displayed in Fig. 5. Our results indicate that UV-weathering expands the environmental window under which aggregation-facilitated removal of MP particles from the aqueous phase occurs. Although the sedimentation rate slightly decreased, these findings suggest that environmental factors such as UV exposure could enhance the interaction of MP with various natural particles, not limited to iron (oxy)hydroxides.

In the environment, the resulting degradation products will be quickly distributed in larger water bodies, unlike in our laboratory experiments. Furthermore, the number of naturally occurring particles is by far larger than the one of MP particles.[53] Considering these two factors, the direct interaction of MP degradation products and MP particles themselves is unlikely in natural settings. Instead, we propose that MP degradation products, measured as DOC fraction, strongly interact with environmental particles either through electrostatic or specific interactions (*e.g.* hydrogen bonding). Hence, under real environmental conditions, MP degradation products may become part of the natural DOC fraction adsorbing to iron (oxy)hydroxides[54,55] and forming iron-DOC flocs[55,56] which might be transported as environmental colloids affecting the overall fate of MP particles.

In future research, it remains to be tested to what extent the findings made for 1 μm PS beads in our experiments can be generalized for a broad range of MP particles with diverse properties (type of polymer, size, shape, density *etc.*).

Data availability

The datasets used in this study are published on Zenodo at **https://doi.org/10.5281/zenodo.14012906**.

Conflicts of interest

There are no conflicts to declare.

Acknowledgements

The study was funded by the Deutsche Forschungsgemeinschaft (DFG, German Research Foundation) – Project Number 391977956 – SFB 1357. The authors would like to thank Dr Ulrich Mansfeld and Martina Heider for taking SEM images at the Bavarian Polymer Institute (BPI).

References

1 M. A. Browne, P. Crump, S. J. Niven, E. Teuten, A. Tonkin, T. Galloway and R. Thompson, Accumulation of microplastic on shorelines worldwide: sources and sinks, *Environ. Sci. Technol.*, 2011, **45**, 9175–9179.

2 A. Cózar, F. Echevarría, J. I. González-Gordillo, X. Irigoien, B. Úbeda, S. Hernández-León, Á. T. Palma, S. Navarro, J. García-de-Lomas, A. Ruiz, M. L. Fernández-de-Puelles and C. M. Duarte, Plastic debris in the open ocean, *Proc. Natl. Acad. Sci. U. S. A.*, 2014, **111**, 10239–10244.

3 D. Eerkes-Medrano, R. C. Thompson and D. C. Aldridge, Microplastics in freshwater systems: a review of the emerging threats, identification of knowledge gaps and prioritisation of research needs, *Water Res.*, 2015, **75**, 63–82.

4 A. A. Horton, A. Walton, D. J. Spurgeon, E. Lahive and C. Svendsen, Microplastics in freshwater and terrestrial environments: evaluating the current understanding to identify the knowledge gaps and future research priorities, *Sci. Total Environ.*, 2017, **586**, 127–141.

5 M. Scheurer and M. Bigalke, Microplastics in Swiss Floodplain Soils, *Environ. Sci. Technol.*, 2018, **52**, 3591–3598.

6 K. A. V. Zubris and B. K. Richards, Synthetic fibers as an indicator of land application of sludge, *Environ. Pollut.*, 2005, **138**, 201–211.

7 R. Dris, J. Gasperi, M. Saad, C. Mirande and B. Tassin, Synthetic fibers in atmospheric fallout: a source of microplastics in the environment?, *Mar. Pollut. Bull.*, 2016, **104**, 290–293.

8 L. Cai, J. Wang, J. Peng, Z. Tan, Z. Zhan, X. Tan and Q. Chen, Characteristic of microplastics in the atmospheric fallout from Dongguan city, China: preliminary research and first evidence, *Environ. Sci. Pollut. Res.*, 2017, **24**, 24928–24935.

9 A. Kelly, D. Lannuzel, T. Rodemann, K. M. Meiners and H. J. Auman, Microplastic contamination in east Antarctic sea ice, *Mar. Pollut. Bull.*, 2020, **154**, 111130.

10 SAPEA, *A Scientific Perspective on Microplastics in Nature and Society*, SAPEA, Science Advice for Policy by European Academies, Berlin, 2019.

11 S. Lambert and M. Wagner, in *Freshwater Microplastics: Emerging Environmental Contaminants?*, ed. M. Wagner and S. Lambert, Springer International Publishing, Cham, 2018, pp. 1–23.

12 L. Persson, B. M. Carney Almroth, C. D. Collins, S. Cornell, C. A. de Wit, M. L. Diamond, P. Fantke, M. Hassellöv, M. MacLeod, M. W. Ryberg, P. Søgaard Jørgensen, P. Villarrubia-Gómez, Z. Wang and M. Z. Hauschild, Outside the Safe Operating Space of the Planetary Boundary for Novel Entities, *Environ. Sci. Technol.*, 2022, **56**, 1510–1521.

13 L. Cai, L. Hu, H. Shi, J. Ye, Y. Zhang and H. Kim, Effects of inorganic ions and natural organic matter on the aggregation of nanoplastics, *Chemosphere*, 2018, **197**, 142–151.

14 S. Li, H. Liu, R. Gao, A. Abdurahman, J. Dai and F. Zeng, Aggregation kinetics of microplastics in aquatic environment: complex roles of electrolytes, pH, and natural organic matter, *Environ. Pollut.*, 2018, **237**, 126–132.

15 A. Pradel, S. Ferreres, C. Veclin, H. El Hadri, M. Gautier, B. Grassl and J. Gigault, Stabilization of Fragmental Polystyrene Nanoplastic by Natural Organic Matter: Insight into Mechanisms, *ACS ES&T Water*, 2021, **1**, 1198–1208.

16 J. Schmidtmann, H. Elagami, B. S. Gilfedder, J. H. Fleckenstein, G. Papastavrou, U. Mansfeld and S. Peiffer, Heteroaggregation of PS microplastic with ferrihydrite leads to rapid removal of microplastic particles from the water column, *Environ. Sci.: Processes Impacts*, 2022, **24**, 1782–1789.

17 T. T. T. Vu, P. H. Nguyen, T. V. Pham, P. Q. Do, T. T. Dao, A. D. Nguyen, L. Nguyen-Thanh, V. M. Dinh and M. N. Nguyen, Comparative effects of crystalline, poorly crystalline and freshly formed iron oxides on the colloidal properties of polystyrene microplastics, *Environ. Pollut.*, 2022, **306**, 119474.

18 O. Oriekhova and S. Stoll, Heteroaggregation of nanoplastic particles in the presence of inorganic colloids and natural organic matter, *Environ. Sci.: Nano*, 2018, **5**, 792–799.

19 F. Lagarde, O. Olivier, M. Zanella, P. Daniel, S. Hiard and A. Caruso, Microplastic interactions with freshwater microalgae: hetero-aggregation and changes in plastic density appear strongly dependent on polymer type, *Environ. Pollut.*, 2016, **215**, 331–339.

20 M. Long, B. Moriceau, M. Gallinari, C. Lambert, A. Huvet, J. Raffray and P. Soudant, Interactions between microplastics and phytoplankton aggregates: impact on their respective fates, *Mar. Chem.*, 2015, **175**, 39–46.

21 J. Michels, A. Stippkugel, M. Lenz, K. Wirtz and A. Engel, Rapid aggregation of biofilm-covered microplastics with marine biogenic particles, *Proc. R. Soc. B*, 2018, **285**, 20181203.

22 Y. Liu, Z. Huang, J. Zhou, J. Tang, C. Yang, C. Chen, W. Huang and Z. Dang, Influence of environmental and biological macromolecules on aggregation kinetics of nanoplastics in aquatic systems, *Water Res.*, 2020, **186**, 116316.

23 N. Singh, E. Tiwari, N. Khandelwal and G. K. Darbha, Understanding the stability of nanoplastics in aqueous environments: effect of ionic strength, temperature, dissolved organic matter, clay, and heavy metals, *Environ. Sci.: Nano*, 2019, **6**, 2968–2976.

24 X. Wang, N. Bolan, D. C. W. Tsang, S. Binoy, L. Bradney and Y. Li, A review of microplastics aggregation in aquatic

environment: influence factors, analytical methods, and environmental implications, *J. Hazard. Mater.*, 2021, 123496.
25 S. Lu, K. Zhu, W. Song, G. Song, D. Chen, T. Hayat, N. S. Alharbi, C. Chen and Y. Sun, Impact of water chemistry on surface charge and aggregation of polystyrene microspheres suspensions, *Sci. Total Environ.*, 2018, **630**, 951–959.
26 Y. Zhang, Y. Luo, X. Yu, D. Huang, X. Guo and L. Zhu, Aging significantly increases the interaction between polystyrene nanoplastic and minerals, *Water Res.*, 2022, **219**, 118544.
27 N. Meides, T. Menzel, B. Poetzschner, M. G. J. Löder, U. Mansfeld, P. Strohriegl, V. Altstaedt and J. Senker, Reconstructing the Environmental Degradation of Polystyrene by Accelerated Weathering, *Environ. Sci. Technol.*, 2021, **55**, 7930–7938.
28 T. Menzel, N. Meides, A. Mauel, U. Mansfeld, W. Kretschmer, M. Kuhn, E. M. Herzig, V. Altstädt, P. Strohriegl, J. Senker and H. Ruckdäschel, Degradation of low-density polyethylene to nanoplastic particles by accelerated weathering, *Sci. Total Environ.*, 2022, **826**, 154035.
29 N. Meides, A. Mauel, T. Menzel, V. Altstädt, H. Ruckdäschel, J. Senker and P. Strohriegl, Quantifying the fragmentation of polypropylene upon exposure to accelerated weathering, *Microplast. Nanoplast.*, 2022, **2**, 23.
30 J. Duan, N. Bolan, Y. Li, S. Ding, T. Atugoda, M. Vithanage, B. Sarkar, D. C. W. Tsang and M. B. Kirkham, Weathering of microplastics and interaction with other coexisting constituents in terrestrial and aquatic environments, *Water Res.*, 2021, **196**, 117011.
31 P. Joshi and A. Kappler, in *Encyclopedia of Astrobiology*, ed. M. Gargaud, W. M. Irvine, R. Amils, P. Claeys, H. J. Cleaves, M. Gerin, D. Rouan, T. Spohn, S. Tirard and M. Viso, Springer, Berlin, Heidelberg, 2020, pp. 1–4.
32 U. Schwertmann and R. M. Cornell, *Iron Oxides in the Laboratory: Preparation and Characterization*, John Wiley & Sons Ltd, Weinheim, 2000.
33 A. Kappler, C. Bryce, M. Mansor, U. Lueder, J. M. Byrne and E. D. Swanner, An evolving view on biogeochemical cycling of iron, *Nat. Rev. Microbiol.*, 2021, **19**, 360–374.
34 J. Wang, X. Zhao, A. Wu, Z. Tang, L. Niu, F. Wu, F. Wang, T. Zhao and Z. Fu, Aggregation and stability of sulfate-modified polystyrene nanoplastics in synthetic and natural waters, *Environ. Pollut.*, 2020, 114240.
35 Y. Li, X. Wang, W. Fu, X. Xia, C. Liu, J. Min, W. Zhang and J. C. Crittenden, Interactions between nano/micro plastics and suspended sediment in water: implications on aggregation and settling, *Water Res.*, 2019, **161**, 486–495.
36 R. M. Cornell and U. Schwertmann, *The Iron Oxides: Structure, Properties, Reactions, Occurrences and Uses*, John Wiley & Sons, 2003.
37 P. Pfohl, M. Wagner, L. Meyer, P. Domercq, A. Praetorius, T. Hüffer, T. Hofmann and W. Wohlleben, Environmental Degradation of Microplastics: How to Measure Fragmentation Rates to Secondary Micro- and Nanoplastic Fragments and Dissociation into Dissolved Organics, *Environ. Sci. Technol.*, 2022, **56**, 11323–11334.
38 J. Schmidtmann and S. Peiffer, A rapid method to quantify sub-micrometer polystyrene particles in aqueous model systems by TOC analysis, *Microplast. Nanoplast.*, 2024, **4**, 3.
39 M. Kosmulski, Isoelectric points and points of zero charge of metal (hydr)oxides: 50 years after Parks' review, *Adv. Colloid Interface Sci.*, 2016, **238**, 1–61.
40 J. Liu, S. M. Louie, C. Pham, C. Dai, D. Liang and Y. Hu, Aggregation of ferrihydrite nanoparticles: effects of pH, electrolytes,and organics, *Environ. Res.*, 2019, **172**, 552–560.
41 Z. Liu, Y. Zhu, S. Lv, Y. Shi, S. Dong, D. Yan, X. Zhu, R. Peng, A. A. Keller and Y. Huang, Quantifying the Dynamics of Polystyrene Microplastics UV-Aging Process, *Environ. Sci. Technol. Lett.*, 2022, **9**, 50–56.
42 Y. Liu, Y. Hu, C. Yang, C. Chen, W. Huang and Z. Dang, Aggregation kinetics of UV irradiated nanoplastics in aquatic environments, *Water Res.*, 2019, **163**, 114870.
43 J. Liu, T. Zhang, L. Tian, X. Liu, Z. Qi, Y. Ma, R. Ji and W. Chen, Aging Significantly Affects Mobility and Contaminant-Mobilizing Ability of Nanoplastics in Saturated Loamy Sand, *Environ. Sci. Technol.*, 2019, **53**, 5805–5815.
44 Y. Wang, X. Chen, F. Wang and N. Cheng, Influence of typical clay minerals on aggregation and settling of pristine and aged polyethylene microplastics, *Environ. Pollut.*, 2023, **316**, 120649.
45 M. Völkl, V. Jérôme, A. Weig, J. Jasinski, N. Meides, P. Strohriegl, T. Scheibel and R. Freitag, Pristine and artificially-aged polystyrene microplastic particles differ in regard to cellular response, *J. Hazard. Mater.*, 2022, **435**, 128955.
46 C. P. Ward, C. J. Armstrong, A. N. Walsh, J. H. Jackson and C. M. Reddy, Sunlight Converts Polystyrene to Carbon Dioxide and Dissolved Organic Carbon, *Environ. Sci. Technol. Lett.*, 2019, **6**, 669–674.
47 P. Möhlenkamp, A. Purser and L. Thomsen, Plastic microbeads from cosmetic products: an experimental study of their hydrodynamic behaviour, vertical transport and resuspension in phytoplankton and sediment aggregates, *Elem. Sci. Anth.*, 2018, **6**, 61.
48 R. Leiser, G.-M. Wu, T. R. Neu and K. Wendt-Potthoff, Biofouling, metal sorption and aggregation are related to sinking of microplastics in a stratified reservoir, *Water Res.*, 2020, 115748.
49 R. Leiser, R. Jongsma, I. Bakenhus, R. Möckel, B. Philipp, T. R. Neu and K. Wendt-Potthoff, Interaction of cyanobacteria with calcium facilitates the sedimentation of microplastics in a eutrophic reservoir, *Water Res.*, 2021, **189**, 116582.
50 P. Liu, X. Zhan, X. Wu, J. Li, H. Wang and S. Gao, Effect of weathering on environmental behavior of microplastics: properties, sorption and potential risks, *Chemosphere*, 2020, **242**, 125193.
51 F. Wang, C. S. Wong, D. Chen, X. Lu, F. Wang and E. Y. Zeng, Interaction of toxic chemicals with microplastics: a critical review, *Water Res.*, 2018, **139**, 208–219.
52 B. Gewert, M. Plassmann, O. Sandblom and M. MacLeod, Identification of chain scission products released to water

by plastic exposed to ultraviolet light, *Environ. Sci. Technol. Lett.*, 2018, **5**, 272–276.

53 A. A. Koelmans, P. E. Redondo-Hasselerharm, N. H. M. Nor, V. N. de Ruijter, S. M. Mintenig and M. Kooi, Risk assessment of microplastic particles, *Nat. Rev. Mater.*, 2022, **7**, 138–152.

54 B. Gu, T. L. Mehlhorn, L. Liang and J. F. McCarthy, Competitive adsorption, displacement, and transport of organic matter on iron oxide: I. Competitive adsorption, *Geochim. Cosmochim. Acta*, 1996, **60**, 1943–1950.

55 E. L. Sharp, P. Jarvis, S. A. Parsons and B. Jefferson, The Impact of Zeta Potential on the Physical Properties of Ferric–NOM Flocs, *Environ. Sci. Technol.*, 2006, **40**, 3934–3940.

56 I. G. Droppo, G. G. Leppard, D. T. Flannigan and S. N. Liss, The Freshwater Floc: A Functional Relationship of Water and Organic and Inorganic Floc Constituents Affecting Suspended Sediment Properties, *Water, Air, Soil Pollut.*, 1997, **99**, 43–54.

